AFRL-RW-EG-TR-2018-029

Simulation-Driven Experiments of Macroscale Explosive Dispersal of Particles

Kyle T. Hughes **Raphael Haftka**
Chanyong Park **S. Balachandar**
Nam-Ho Kim

University of Florida
Department of Mechanical and Aerospace Engineering
Gainesville, FL 32611

Angela Diggs
Don Littrell

Air Force Research Laboratory
Munitions Directorate/Ordnance Division
Damage Mechanisms Branch (AFRL/RWMW)
Eglin AFB, FL 32542-6810

April 2018

Final Report for April 2016 – January 2018

Distribution A: Approved for public release; distribution unlimited.
Approval Confirmation 96TW-2017-0471 dated 22 December 2017

AIR FORCE RESEARCH LABORATORY
MUNITIONS DIRECTORATE

■ Air Force Materiel Command ■ United States Air Force ■ Eglin Air Force Base, FL 32542

NOTICE AND SIGNATURE PAGE

Using Government drawings, specifications, or other data included in this document for any purpose other than Government procurement does not in any way obligate the U.S. Government. The fact that the Government formulated or supplied the drawings, specifications, or other data does not license the holder or any other person or corporation; or convey any rights or permission to manufacture, use, or sell any patented invention that may relate to them.

Qualified requestors may obtain copies of this report from the Defense Technical Information Center (DTIC) (http://www.dtic.mil/dtic/index.html).

AFRL-RW-EG-TR-2018-029 HAS BEEN REVIEWED AND IS APPROVED FOR PUBLICATION IN ACCORDANCE WITH ASSIGNED DISTRIBUTION STATEMENT.

FOR THE DIRECTOR:

=Signed=	*=Signed=*
JOHN D. CORLEY. PhD	ANGELA S. DIGGS
Ordnance Sciences	Program Manager
Core Technical Competency Lead	Damage Mechanisms Branch
Ordnance Division	

This report is published in the interest of scientific and technical information exchange, and its publication does not constitute the Government's approval or disapproval of its ideas or findings.

This page intentionally left blank

REPORT DOCUMENTATION PAGE

Form Approved
OMB No. 0704-0188

Public reporting burden for this collection of information is estimated to average 1 hour per response, including the time for reviewing instructions, searching existing data sources, gathering and maintaining the data needed, and completing and reviewing this collection of information. Send comments regarding this burden estimate or any other aspect of this collection of information, including suggestions for reducing this burden to Department of Defense, Washington Headquarters Services, Directorate for Information Operations and Reports (0704-0188), 1215 Jefferson Davis Highway, Suite 1204, Arlington, VA 22202-4302. Respondents should be aware that notwithstanding any other provision of law, no person shall be subject to any penalty for failing to comply with a collection of information if it does not display a currently valid OMB control number. **PLEASE DO NOT RETURN YOUR FORM TO THE ABOVE ADDRESS.**

1. REPORT DATE (DD-MM-YYYY)	2. REPORT TYPE	3. DATES COVERED (From - To)
13 April 2018	Final	April 2016 – January 2018

4. TITLE AND SUBTITLE

Simulation-Driven Experiments of Macroscale Explosive Dispersal of Particles

5a. CONTRACT NUMBER

5b. GRANT NUMBER

5c. PROGRAM ELEMENT NUMBER
62602F

6. AUTHOR(S)
Kyle T. Hughes, Chanyong Park, Nam-Ho Kim, Raphael Haftka, S. Balachandar, Angela Diggs, Don Littrell

5d. PROJECT NUMBER
25029992

5e. TASK NUMBER

5f. WORK UNIT NUMBER
W10Y

7. PERFORMING ORGANIZATION NAME(S) AND ADDRESS(ES)
Air Force Research Laboratory, Munitions Directorate
Ordnance Division
Damage Mechanisms Branch (AFRL/RWMW)
Eglin AFB FL 32542-5430

8. PERFORMING ORGANIZATION REPORT NUMBER

9. SPONSORING / MONITORING AGENCY NAME(S) AND ADDRESS(ES)
Air Force Research Laboratory, Munitions Directorate
Ordnance Division
Damage Mechanisms Branch (AFRL/RWMW)
Eglin AFB FL 32542-5430
Technical Advisor: Joel W. House, PhD

10. SPONSOR/MONITOR'S ACRONYM(S)
AFRL-RW-EG

11. SPONSOR/MONITOR'S REPORT NUMBER(S)
AFRL-RW-EG-TR-2018-029

12. DISTRIBUTION / AVAILABILITY STATEMENT
Distribution A: Approved for public release; distribution unlimited. Approval Confirmation 96TW-2017-0471, dated 22 December 2017

13. SUPPLEMENTARY NOTES

14. ABSTRACT
A series of explosive tests were completed at the Air Force Research Laboratory's blastpad facility. The six test articles include two bare charges of Composition B, three charges surrounded by an annulus of fine steel powder, and one charge surrounded by an annulus of fine tungsten powder. The experimental instrumentation includes four high-speed cameras from various viewpoints, fifty-four pressure transducers flush-mounted radially around the charge, six cylindrical momentum traps, and optical linear encoders. The objective of the test series is to enable validation efforts for high fidelity multiphase models being developed at the University of Florida Center for Compressible Multiphase Turbulence. The analysis included here enables an uncertainty analysis for the baseline bare charge configuration using current and legacy data. Additionally, pre-scoring the case for the multiphase liner shots was shown to have no discernible effect on the particle-gas instabilities observed. Preliminary data analysis is performed, with emphasis on the shock location time of arrival, peak pressure values, and high speed video analysis. Additional analysis and comparison to simulation results will be performed in future efforts.

15. SUBJECT TERMS
multiphase blast, modeling and simulation, experiment, uncertainty quantification

16. SECURITY CLASSIFICATION OF:			17. LIMITATION OF ABSTRACT	18. NUMBER OF PAGES	19a. NAME OF RESPONSIBLE PERSON
a. REPORT	b. ABSTRACT	c. THIS PAGE			Angela S. Diggs
UNCLASSIFIED	UNCLASSIFIED	UNCLASSIFIED	SAR	28	19b. TELEPHONE NUMBER (include area code)

Standard Form 298 (Rev. 8-98)
Prescribed by ANSI Std. Z39.18

This page intentionally left blank

Table of Contents

List of Figures

Figure **Page**

List of Figures (con't)

Figure **Page**

List of Tables

Table **Page**

I. INTRODUCTION

The experiments in this investigation were to designed to validate the high-fidelity, multiphase models developed by the University of Florida (UF) Center of Compressible Multiphase Turbulence (CCMT). The experimental validation test is a high speed dispersal of an annular particle bed driven by a core of reacting explosive. Many interesting and complex phenomena are present in the experiment, including detonation chemistry, turbulence, particle collisions, drag forces, real gas effects, shock-particle interactions, and particle-contact interactions. These experiments serve as validation for multiphase models developed to predict the shock front location, particle front location, and instabilities arising in the particle cloud. Additionally, the uncertainty in the experimental inputs were quantified for use in the simulation validation effort.

It is extremely challenging to validate the complex flow associated with explosive particle dispersal. It can be beneficial to separate the problem into a set of simpler experiments that isolate the relavant physics, as recommended by Oberkampf[1]. Accordingly, at the CCMT and within the general multiphase community the philosophy has been to break the problem of explosive dispersal of particles into simplifying conditions, typically by using a multiscaling approach that reduces the number of particles considered. The microscale, mesoscale, and macroscale are identified by the total number of particles, where the lower scales may be used to provide insight into the larger scales. Previous investigations have considered explosive particle dispersion at the microscale; this effort focuses on the macroscale investigation that builds upon that knowledge.

Microscale refers to investigations where approximately O(1) to O(10^4) particles are present. In microscale simulations, few particles are considered to allow the fine details of the flow to be resolved with high fidelity, such as the flow around each individual particle. In microscale experiments, the particle positions, velocities, and forces may be extracted for individual particles. Experiments by Takayama and co-workers[2–4] used an accelerometer installed inside the sphere to measure the force on the particle on sub-microsecond resolution. Various investigators have also conducted microscale experiments in shock tubes where an isolated or a small collection of particles are allowed to move freely in response to forces exerted on them by the shock and the post-shock flow[5–7]. Hughes et al.[8] tracked the position of a small number of particles subjected to a detonation wave with the use of X-ray imaging.

The mesoscale regime is an intermediate regime that refers to investigations where O(10^5) to O(10^8) particles are present. The mesoscale regime is characterized by significantly increased computational expense in simulations and the fully-resolved flow field around the particle is often exchanged for point particle approximations or adoption of a two-fluid model. While it is still possible in this regime for each computational particle to correspond to a physical particle, an approximation is often made to consider a cloud of physical particles as a single computational particle, where super-particle loading quantifies the number of physical particles represented by a single computational particle. Physically, the mesoscale regime is also where instabilities may begin to manifest. Experimentally, the large number of particles are usually characterized in terms of fronts and volume fractions, with only average quantities for drag extracted. Wagner and colleagues[9,10] have conducted various investigations studying particle curtains interacting with a planar shock wave within a shock tube. Particle fronts were extracted with high-speed schlieren photography while time-varying particle curtain volume fraction was obtained from x-ray imagery. Kellenberger et al.[11] performed similar investigations with increased volume fraction and a stationary fixed bed of particles.

The largest regime is the macroscale, which is characterized by greater than $O(10^9)$ particles. The macroscale regime is usually representative of a realistic engineering application. Computationally, it is too expensive within this regime to resolve all the particles, even when the particles are represented as point particles; thus the super-particle loading is required for macroscale simulations. High fidelity data for explosive particle dispersal at the macroscale is limited in the literature due to the diagnostic equipment available, extreme environment during detonation, and relatively high experimental cost. Frost, Zhang, and collaborators have conducted a series of exploratory experiments under varying test configurations to understand the nature of explosive dispersal of particles and the resulting instabilities of the rapidly advancing particle front through high-speed video analysis.[12–15]

However, the exploratory nature of those experiments provides limited data for validation of high-fidelity multiphase simulations. The current experiments were designed to provide validation quality data for high-fidelity simulations by including a wide array of instrumentation to quantify the behavior of the gas, particles, and combined gas-particle flow. In addition, the experiments were designed to meet simulation capabilities and limitations of the CCMT. For example, the CCMT models are not capable of simulating fragmentation of the case material used to contain the particles. Therefore, the experiment was designed to use a thin case material to reduce the energy and effect of the case fragmentation on the flow. In addition, possible sources of uncertainty have been compiled through extensive discussion between simulation and experimental teams and, where possible, these sources of uncertainty have been addressed a priori.

II. EXPERIMENTAL SETUP

The macroscale experiments were conducted at the Air Force Research Laboratory (AFRL) blastpad, shown in Figure 1. The blastpad is an outdoor testing facility located at Eglin Air Force Base (AFB) with an instrument suite including 54 in-ground Kulite HKS-37-375 series pressure transducers and four high speed cameras. The test charge is oriented horizontally with the center axis placed flush with the ground. The charge is supported with a wooden frame and a Styrofoam cradle. When the test charge is detonated, the lower half of the resulting detonation is directed downward, turned, and then exhausts to a pit away from the Blastpad (see Barreto et al.[16] for further details concerning the AFRL blastpad); the lower half of the charge is not expected to contribute to or interfere with the data collection on the blastpad. The complementary simulation is a 3D slice of the flow field located on the 90-degree line (camera 3 axis in Figure 1). The following paragraphs detail the experimental setup and explain how the simulation capabilities affected test design.

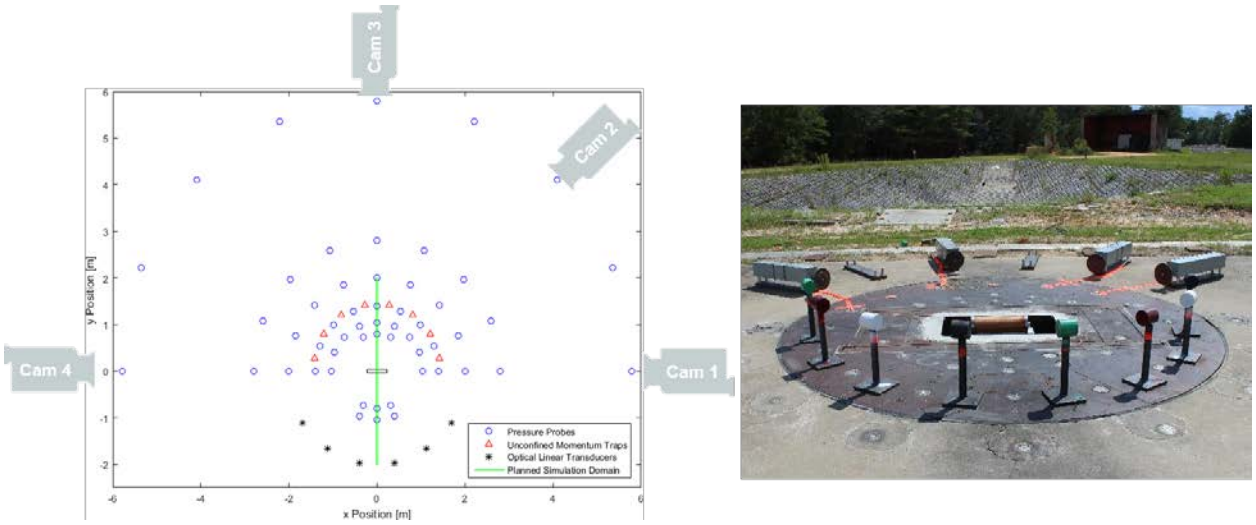

a) b)

Figure 1. Details of the macroscale experiments. a) Locations of the test instrumentation relative to the test charge, b) Close up view of a test charge suspended above the exhaust ducting; exhaust pit shown in background

A schematic of the explosive charge with a particle liner is presented in Figure 2a. Results published in the literature suggest that the casing fragmentation is highly correlated with the number of jets appearing in the macroscale problem[17]. However, because the case material was designed to minimize the energy required for case fragmentation, the case is not expected to drive the jetting behavior in the current test. The test articles were designed with an annular structure that has no inner casing between the pressed Composition B explosive and the particle bed. Additionally, 3/16" phenolic tubing was chosen as the outer case wall with a set number of pre-scored notches traveling the long axis of the test article (see Figure 2b). The notches serve to weaken the case structure at pre-determined locations. Though the notches are not expected to drive the case fragmentation or gas-particle jetting behavior, they are included for completeness. If the observed jetting is correlated to the number and location of the notches, then it will be a strong indicator that case fragmentation is a major player in the flow physics, regardless of the energy required to fragment the case. If true, the simulations would be required to include the case and its fragmentation, which is not currently considered.

Cost constraints limited the number of test shots to six. AFRL had two legacy test shots of bare Composition B charges that could be used for the uncertainty quantification of the baseline configuration; thus two additional bare shots were sufficient for this test series. The four remaining test configurations were planned to consider the effect of a particle liner surrounding the bare charge. To enable analysis of the experimental uncertainty, three of the test articles used a steel particle liner. The fourth configuration uses a tungsten particle liner to provide a quick-look of the effect of changing the particle material properties on the multiphase flow. As noted above, the cases were notched for several configurations, where the final shot configuration is shown below in Table 1.

Table 1. Shot configuration for six test articles

Shot	Liner	Notched?
1	-	-
2	-	-
3	Tungsten	Y
4	Steel	Y
5	Steel	Y
6	Steel	N

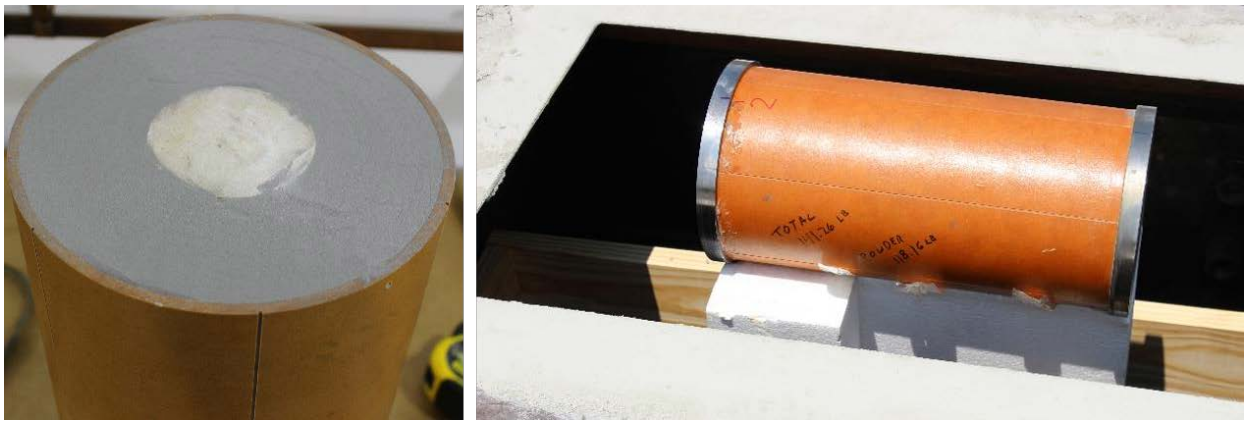

a) **b)**

Figure 2. Macroscale test articles. a) Charge cross-section showing thin outer wall, particles, and explosive; note there is no inner wall between particles and explosive, b) Charge shown suspended above the exhaust tunnel on the wooden frame and Styrofoam cradle

Investigations of explosive dispersal of particles have shown that instabilities will arise for even a bare charge (i.e. one that does not have a layer of particles around the explosive) but will only persist for early times. Charges that contain a layer of particles exhibit jets that persist for significantly longer times[14]. Furthermore, those investigations show that large instability waves persisting for long times[12,13,15] when the ratio of the particle mass to the charge mass (M/C ratio) is greater than 10. Therefore, the current multiphase liner test articles were designed with a M/C ratio of 10. Composition B was chosen for its tie-in to AFRL legacy data, processing ease, and high Gurney energy of approximately 2.7 km/s. The Gurney energy may be considered as a measure of the explosives ability to quickly accelerate a surrounding layer of metal[18]. To achieve a M/C ratio of 10, each multiphase liner test article contains 85 lbs (39 kg) of particles (steel or tungsten) surrounding 8.5 lbs of explosive charge. The case outer diameter was determined by assuming a 40% packing fraction, which was realized with the tungsten particles. The steel particles achieved a 60% packing fraction, which led to a final M/C of 13. Schematics of the test configurations can be seen in Figure 3.

Simulations of explosive dispersal must include an appropriate reactive burn model to impart the correct energy into the simulation. Reactive burn model parameters are calibrated using empirical results. The bare charge configurations tested can be used to validate the reactive burn model parameters. The two repeated tests for the bare charge are used in conjunction with the legacy data to validate the reactive burn model implemented in the simulations by comparing pressure fields, shock location, and contact line location.

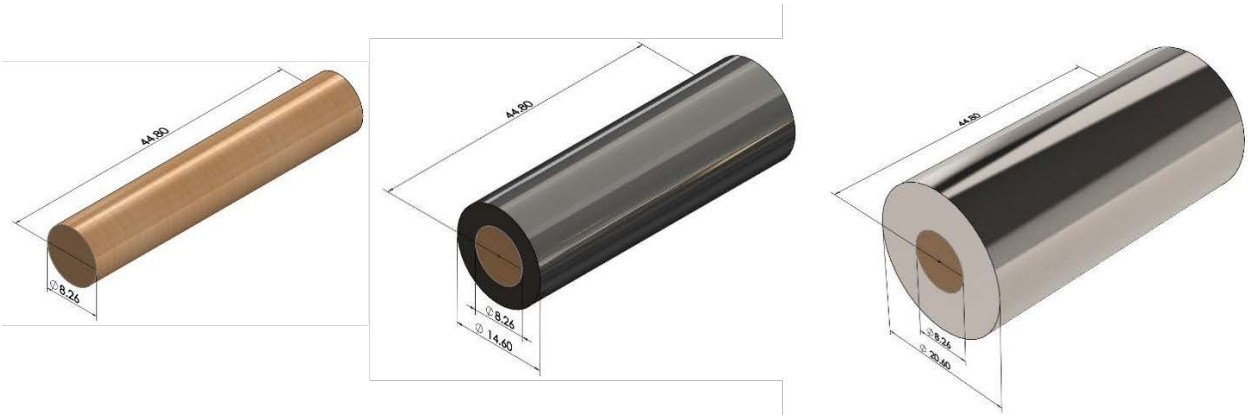

a) b) c)

Figure 3. Test article schematic based on material. a) Bare charge of Composition B with 3.25” diameter and 17.6” length, b) Composition B charge with 1.25” thick tungsten particle liner, c) Composition B charge with 2.43” thick steel particle liner

III. UNCERTAINTY QUANTIFICATION

For the current set of experiments, the generalized framework for uncertainty quantification and validation presented in Hughes et al.[8] may be applied to the macroscale experiments, shown in Figure 4.

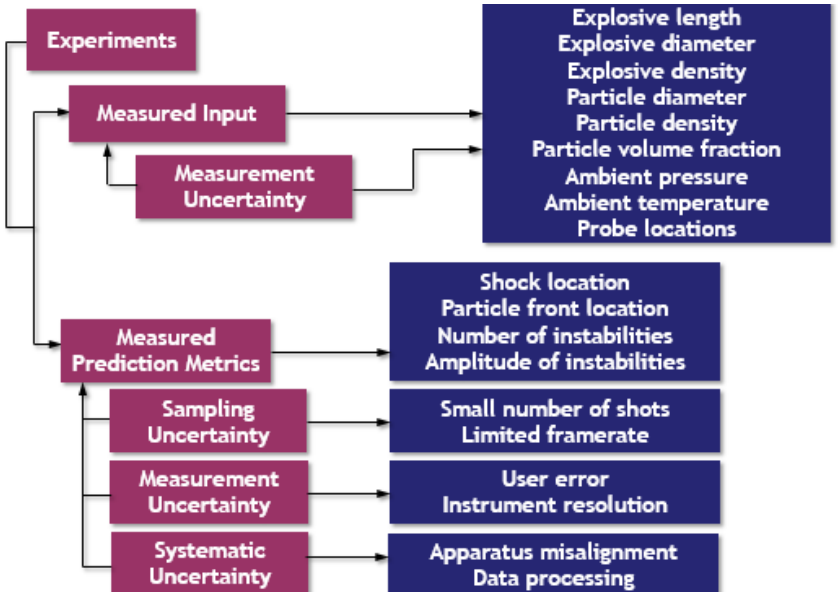

Figure 4. Uncertainty quantification framework used for the macroscale experiments

The Composition B charges were manufactured at the High Explosives Research and Development Facility (HERD) located on Eglin AFB. The HERD measured the diameter and length of the explosive after manufacture, with several diameter measurements along the length to ensure a consistent diameter, see Table 2. A nominal density is also reported in Table 3. In addition, the explosive charges were x-rayed to reveal any significant voids within the explosive (see Figure 5); none were found.

Table 2. Measurements of charge dimensions to assess geometric manufacturing uncertainty

Charge	Diameter (in)						Length (in)
	Bottom	1/4	Mid	3/4	Top	Average	
1	3.225	3.226	3.225	3.23	3.23	3.227	17.63
2	3.223	3.223	3.224	3.226	3.226	3.224	17.63
3	3.224	3.225	3.225	3.224	3.225	3.225	17.63
4	3.223	3.223	3.226	3.226	3.226	3.225	17.62
5	3.225	3.225	3.225	3.226	3.226	3.225	17.60
6	3.23	3.23	3.224	3.225	3.224	3.227	17.63
Average	3.225	3.225	3.225	3.226	3.226	**3.226**	**17.62**
Std Dev	0.003	0.003	0.001	0.002	0.002	0.001	0.01

Table 3. Calculated charge density with comparison to percent theoretical maximum density for Composition B

Charge	Diameter (in)	Length (in)	Volume (cc)	Mass (lb)	Density (g/cc)	% TMD
1	3.227	17.63	2362	9.04	1.736	99.8
2	3.224	17.63	2359	9.01	1.732	99.6
3	3.225	17.63	2359	9.04	1.738	99.9
4	3.225	17.62	2358	9.03	1.737	99.8
5	3.225	17.60	2357	9.06	1.743	100
6	3.227	17.63	2363	9.06	1.739	100.0
Average	3.226	17.62	2360	9.04	1.738	99.8
Std Dev	0.001	0.01	2	0.02	0.004	0.2

Extensive effort was made to obtain steel particles with high sphericity and a narrow particle size range to enable the simulation to assume spherical, monodisperse particles. A narrow size range circumvents the need for time-consuming particle sieving, a significant concern because 85 lbs of steel particles were required per shot. Fifteen vendors were considered, with three selected as prospective candidates to investigate further. Samples were obtained from these three vendors, American Elements, Atlantic Equipment Engineers, and Sandvik Osprey, and examined under the scanning electron microscope (SEM). The results shown in Figure 6 reveal Sandvik Osprey to be the most spherical with the narrowest particle size range.

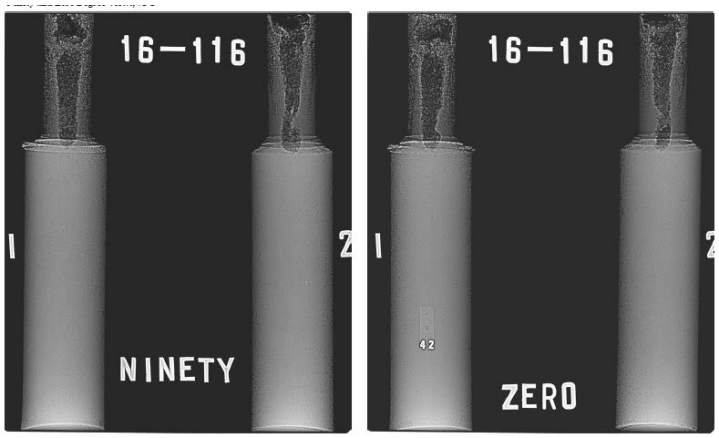

Figure 5. X-ray image of the uncut charges (billets appear at top of the photograph). The x-rays reveal the charges are homogenous with no large voids present

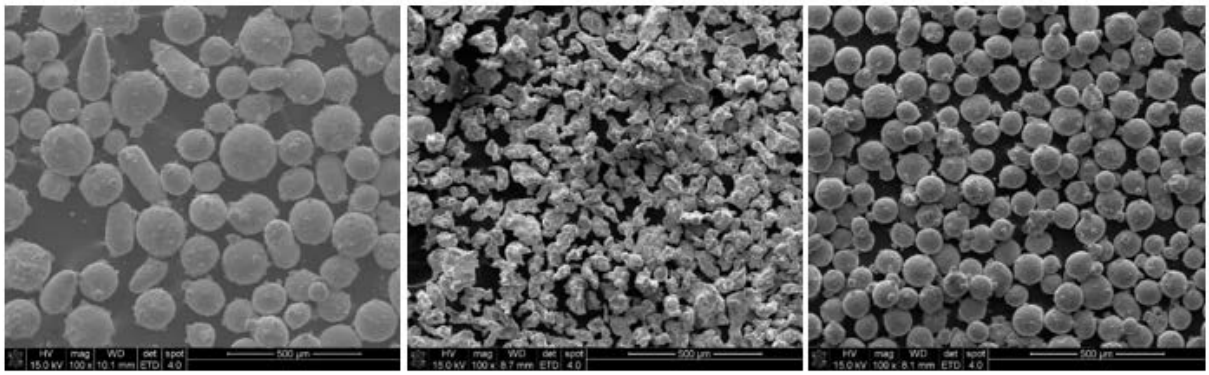

Figure 6. Preliminary characterization of steel particles under SEM. SEM images are labeled with manufacturer and reported size range. Sandvik Osprey provided particles with the highest sphericity and narrowest size range

Particle density has obtained from repeated runs of a Quantrachrome UltraPyc 1000 helium gas pycnometer. The results are compiled in Table 4 for the steel particles.

Table 4. Results of twelve repeated runs in the Quantachrome UltraPyc 1000 helium gas pycnometer for the steel particles

Run	Vol [cc]	Density [g/cc]
1	14.54	7.681
2	14.57	7.664
3	14.59	7.656
4	14.59	7.655
5	14.59	7.654
6	14.59	7.653
7	14.59	7.655
8	14.61	7.646
9	14.59	7.652
10	14.60	7.648
11	14.59	7.652
12	14.60	7.647
Avg	14.59	7.655
Std dev	0.02	0.009

IV. RESULTS

The following section will present results for the pressure probes, particle dispersal visualization, and image analysis. The image analysis is ongoing and will only address the shock time of arrival. Additional effort is ongoing to obtain more advanced prediction metrics such as particle front and instability characterization. Results for the secondary diagnostics such as the unconfined momentum traps and optical linear encoders are deferred to a future publication.

A. Pressure Probe Results

The pressure histories were processed to recover the peak pressure (PP) and the shock time of arrival (TOA). The PP was determined as the first peak encountered by the probe. Some of the pressure histories are subject to large fluctuations due to noise or debris impacting the pressure transducer and have been manually corrected to ensure erroneous peaks were not selected. The pressure histories were subject to a delay before the detonator activates. A Pearson probe recorded the increase in current in the trigger line, shown in Figure 7a. The sudden drop in the Pearson probe signal corresponds to the action of the exploding bridgewire within the detonator. In this example, the delay till initiation is 1.893 ms. The activation of the detonator is considered to be the initial time in all subsequent plots. PP results are reported in gauge pressure. The shock TOA was determined as the time when the pressure reaches 50% of the PP. An example of the PP and TOA are shown in Figure 7b.

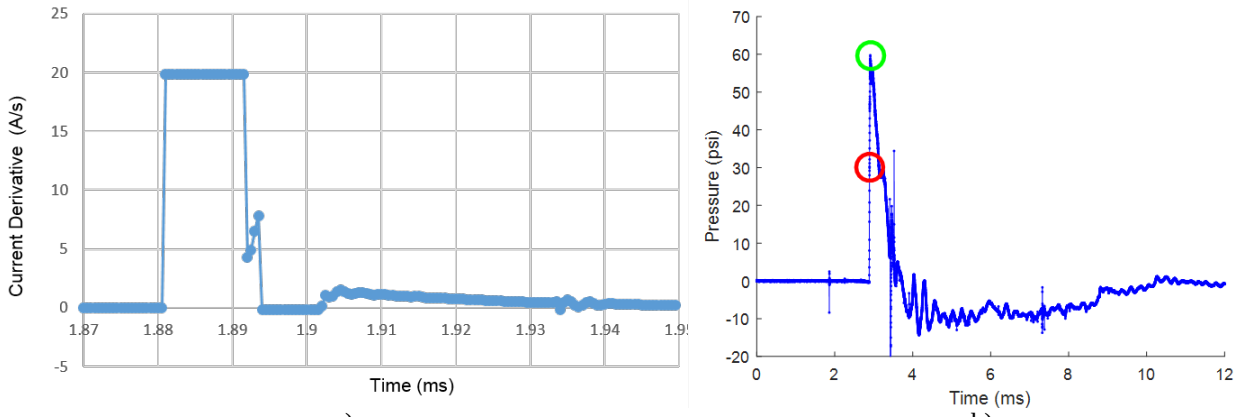

a) b)

Figure 7. Example results for detonator delay, peak pressure, and shock time of arrival. a) Pearson probe results showing the sudden drop in current when the exploding bridgewire within the detonator activates. The example delay shown is 1.893 ms. b) Sample pressure trace showing the selected peak pressure (green) and shock time of arrival (red). The times in the pressure history have not been corrected to account for the detonator delay

PP contours are presented in Figure 8 for each test configuration. Linear interpolation was used between the pressure transducers to construct the pressure field. The bare charge shows local maxima at the 0-degree and 90-degree directions. The 0-degree maximum is due to the explosive burning towards that direction while the 90-degree results from the cylindrical geometry. The tungsten and steel liner shots greatly reduce the PP over the entire measured pressure field. In addition, the 90-degree line no longer experiences a local maximum for the particle liner shots. Instead, the tungsten liner shot greatly smooths out the pressure field compared to the bare charge. The steel liner shot shows a local minimum at the 90-degree line.

For validation of the high fidelity simulations on the centerline, results on the 90-degree line will be presented. Validation of the reactive burn model employed to model the explosive is a major concern for the simulation. Matching the bare charge results for the shock TOA and PP are basic checks for the explosive modeling. The bare charge geometry provides additional repeat tests for UQ in this validation exercise. Figure 9 presents the experimental results along the explosive centerline for the bare charge with the legacy data, where close examination of the data shows no discernible pattern in the results to indicate a bias between the old and new data (though note the log scale!).

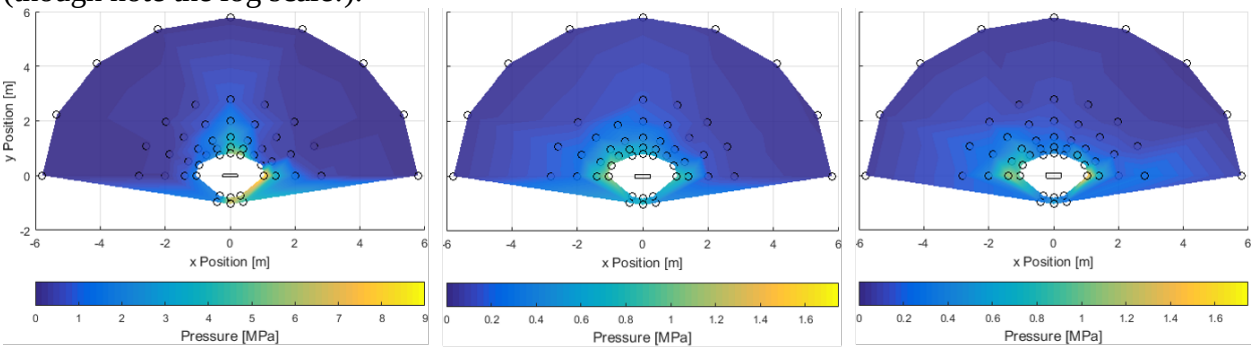

a) Bare charge b) Tungsten liner c) Steel liner

Figure 8. Interpolated pressure fields. a) Pressure field of the bare charge configuration (July 2017 – Shot 1) showing local maxima at the 0-degree and 90-degree lines, b) Pressure field of the tungsten liner configuration (July 2017 – Shot 3), c) Pressure field of the steel liner configuration (July 2017 – Shot 4) showing local minimum at the 0-degree lines

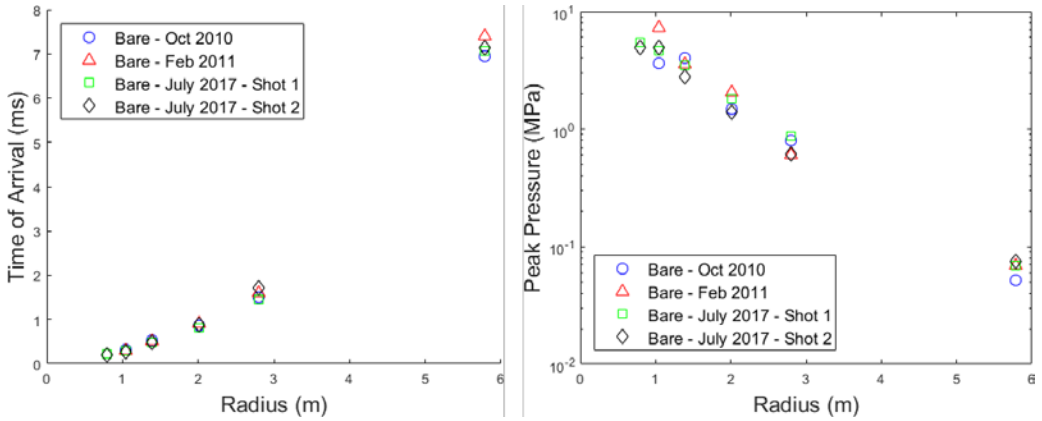

a) b)

Figure 9. Consistency of previous data with new results. Result are presented for the a) shock time of arrival results and b) peak pressure results on the charge centerline for the bare charge configuration

As ntoed, the CCMT simulations cannot model the case, and there are no current plans to add that capability. The case is required to contain the fine particle bed and certainly influences the flow. The experimental results are used to provide evidence that case notching does not affect the time of arrival or peak pressure, as shown for the three repeated steel shots in Figure 10. The results are given along the centerline since this is the region of interest for CCMT simulation validation. The results for shock TOA exhibit very little spread while the PP plot shows a greater, but still small, variation (as shown in the log scale). The spread appears to be random in nature, with no discernible pattern based on case notching. While it is intuitive that the case has an influence on the flow, weakening a case that was designed to require minimum energy to fragment does not appear to effect the shock TOA or PP. Thus the CCMT has confidence in completing the simulations without modeling the case.

The above analysis and discussion of the legacy data and effect of case notching motivates the decision to combine all bare charge shots and all steel liner shots, as shown in Figure 11. The bare charge configuration now contains a sample size of four, the tungsten liner configuration is still a single sample, and the steel liner configuration now contains three samples. The error bars in Figure 11 are equal to one standard deviation for the repeated samples. The shock TOA for the bare charge is especially vital to validation as the image analysis was unable to recover the experimental shock location.

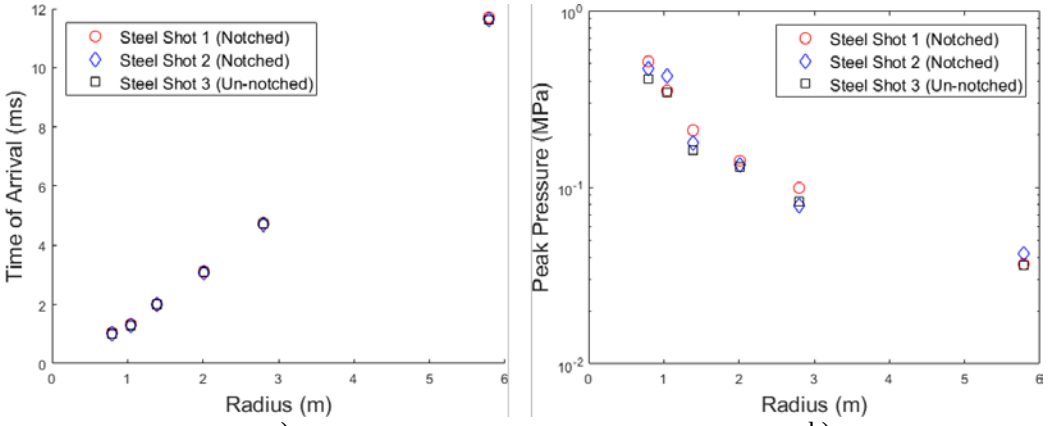

a) b)

Figure 10. Effect of case notching. a) Shock time of arrival results, b) peak pressure results

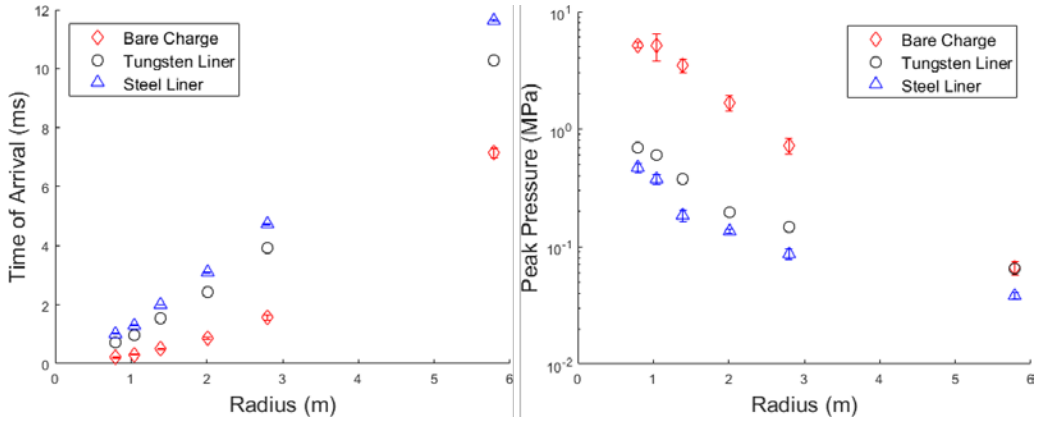

Figure 11. Compilation of pressure probe results. Error bars are one standard deviation. Bare charge (n=4) and steel liner (n=3) configurations are averages while the tungsten is a single sample. a) Shock time of arrival results, b) peak pressure results

B. Particle Dispersal Visualization

Figure 12 shows high-speed imagery of the explosive event for the three different test configurations as viewed from camera 1 (e.g. along the long axis of the cylindrical charge). Note that varying levels of magnification were used for each of the tests shown, and the charge burns towards the viewer from this perspective. The brightly luminescing explosive products of the bare charge saturates the image and prevents identification of the shock location. However, the explosive product front clearly displays the formation of instabilities as it expands.

For the steel and tungsten liner configurations, a dense soot cloud is formed at the end that obscures the initial development of the particle liner. By 1.67 ms, the tungsten particle liner is visible. At 2.42 and 3.76 ms, the tungsten particles are luminescent as they disperse. Some of the tungsten particles seem to track almost simultaneously with the shock front, with a bright, dense band following. After the passage of this bright band, alternating bright and dark striations are present that indicate instabilities in the tungsten particle liner. The steel shot shows different characteristics. Specifically, there is little/no luminescence in the steel particles, and the steel particles appear to travel well behind the shock front. The steel particles exhibit instabilities closer to that shown in the work of Frost and colleagues[13,15], with fine fingers racing ahead of the front. The instabilities, however, are so numerous that they are not easily distinguishable from the next layer of instabilities. Additionally, the amplitude and number of instabilities are not easily measurable.

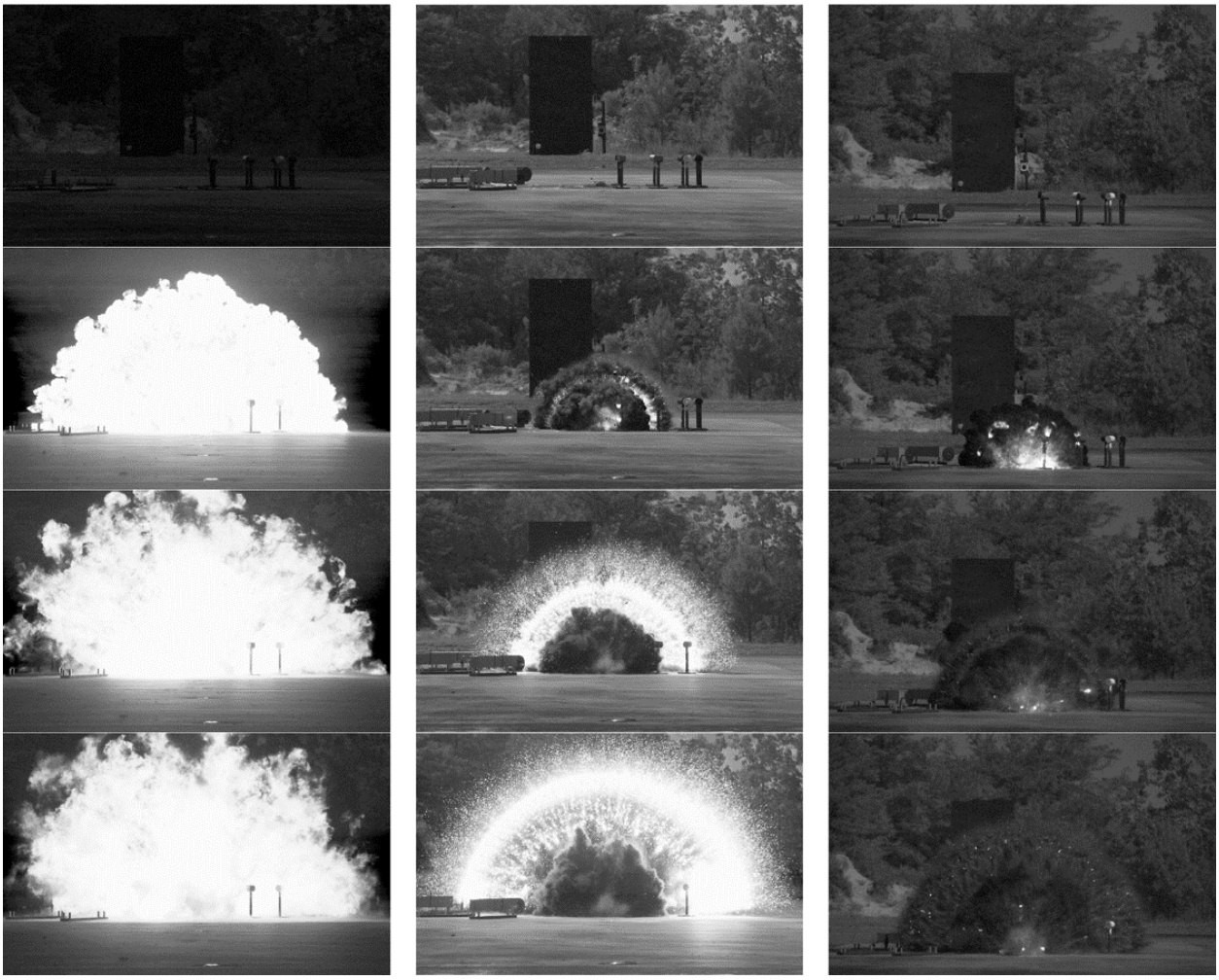

a) Bare charge b) Tungsten liner c) Steel liner

Figure 12. High-speed imagery of the three test configurations obtained from camera 1. Time stamps (from top to bottom) are 0, 1.67, 2.42, and 3.67 ms for a) bare Composition B, b) Composition B with tungsten liner, and c) Composition B with steel liner (note magnifications are not equal for all test conditions)

Figure 13 offers another perspective of the explosive event from the 90-degree view provided by camera 3. The charge is burning from right to left in this image. From this orthogonal perspective, the explosive products are restricted to a fairly narrow band with a fireball traveling in the burn direction with a trailing dark soot cloud. The basic form is repeated in the steel and tungsten liner shots, with the exception that the upstream fireball is occluded by a soot cloud after very early times. The still images of the steel and tungsten liner shot reveal the particles are initially occluded by black soot and casing fragments but emerge as time progresses. The tungsten particles are luminesce such that the brightness of the particle band increases as more particles become visible. While not as easily distinguishable, the steel particles are a characteristic gray color that emerge from the soot cloud. The brightness of the tungsten particles prevent identifying the case fragments, but they are observed in the steel liner shot to break into many fine strips. From the view shown here, approximately 11 strips are present across the roughly 90-degree area visible. A total of approximately 44 strips around the circumference of the casing may be estimated to be present, lending futher credibility to the previous conclusion

that the case notches had no effect. Additionally, the un-notched case in the third steel shot shows similar behavior (not shown below).

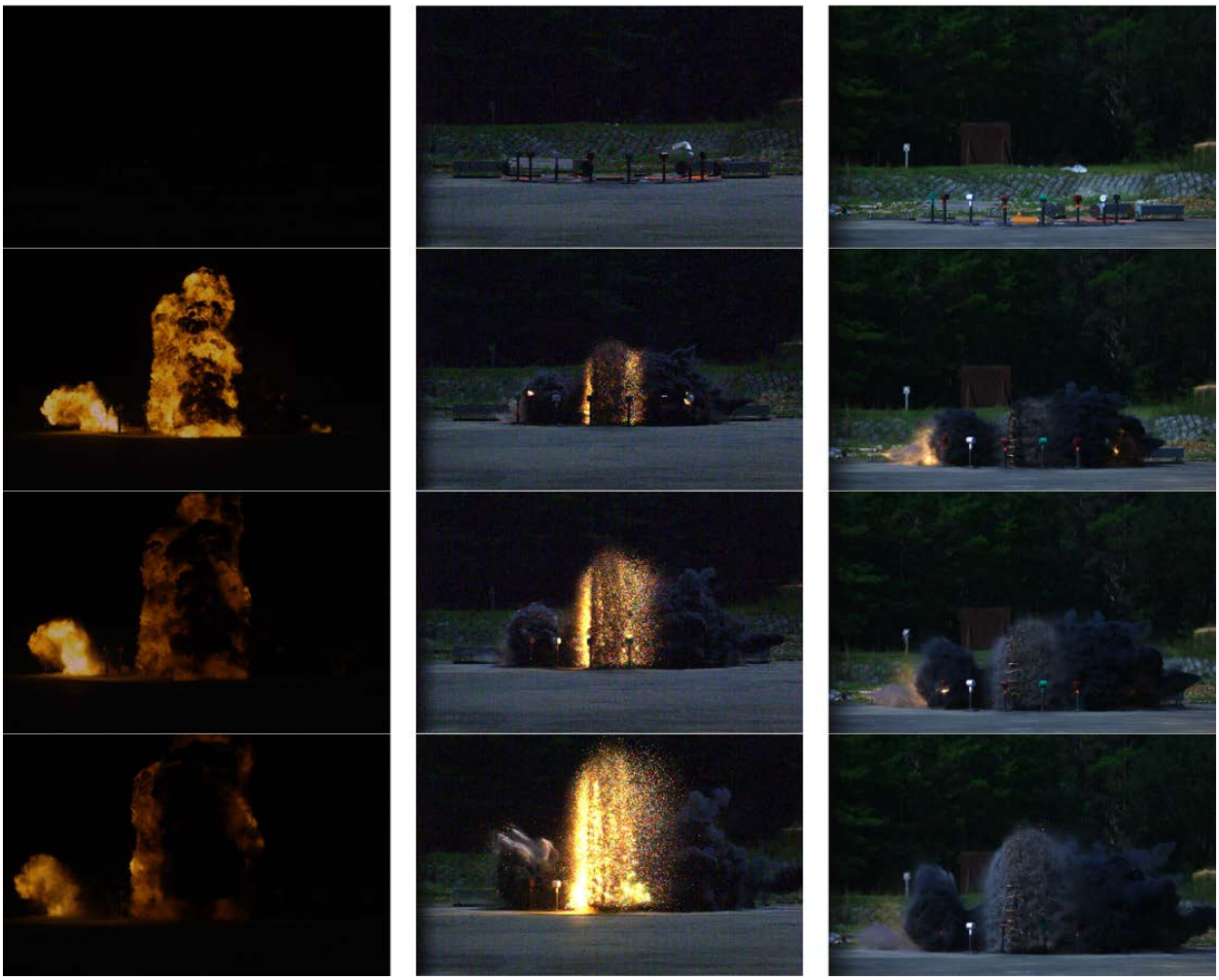

a) Bare charge b) Tungsten liner c) Steel liner

Figure 13. High-speed imagery of the three test configurations obtained from camera 3. Time stamps (from top to bottom) are 0, 1.60, 2.40, and 3.60 ms for a) bare Composition B, b) Composition B with tungsten liner, and c) Composition B with steel liner (note magnifications are not equal for all test conditions)

C. Image Analysis

Capturing the shocks from multiple perspectives was advantageous for simulation validation. The high fidelity simulations to be conducted at CCMT are currently planned as a narrow slice orthogonal to the test article. Furthermore, it is likely that the simulations will be restricted to the first few milliseconds due to computational cost. High-speed imagery from the 90-degree perspective offered by camera 3 reveals that multiple shock fronts are present. If the shock had only been captured from a single camera, such as camera 1 or camera 4, significant bias would have been introduced. The shocks from the ends of the cylinder initially outpace the shock from the center of the cylinder, occluding the location at the centerline. See Figure 14 for an example of this behavior.

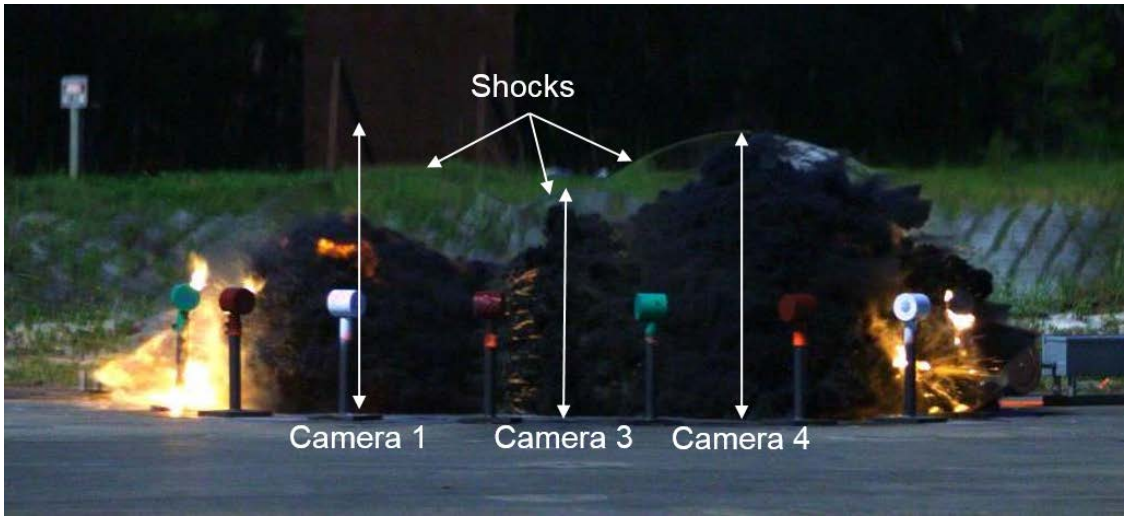

Figure 14. Multiple shock structure visible in the explosive tests. The various perspectives record differing results for the shock location, with cameras 1 and 4 overestimating the shock location at the centerline. The image shown here is from the first steel liner shot, 1.067 ms after detonation

The high speed videos were analyzed manually to determine the shock location with respect to time. Figure 15a shows an example of the pre-shot image containing the calibration fiducial used to establish the spatial resolution for the camera. The fiducial was aligned normal to the camera and each checker in the pattern is nominally 1”x1”. Figure 15b shows an example of the manual selection of the shock for each frame. The previous shock locations are overlaid in green. Low contrast areas sometimes made the shock unrecoverable against the dark background even with image enhancement. At times when the shock location is not clear, the frame is skipped, leading to gaps in the data in the following analysis.

a) b)

Figure 15. Image analysis examples. a) Each camera used a static image with a checker pattern fiducial to calibrate the image. b) The location of the shock was selected manually for each frame along the centerline and normal to the ground. Previous selections are shown as green markers

Figure 16 shows the image analysis results for each of the particle liner shots. Shock tracking results for cameras 1, 3, and 4 have been included along with the shock TOA results from the pressure probes orthogonal to the charge. For the tungsten liner configuration, cameras 1 and 4 appear to better align the pressure probe results. The steel liner configuration shows that camera 3 approximately follows the pressure probes for all but the first shot. Camera 1 in the first steel shot departs from the values produced by camera 4, an unexpected anomaly when comparing the trends of the other three particle liner shots. It is likely that camera 1 has a source of uncertainty

not currently understood. The close agreement between the pressure probes and camera 3 for the steel shot indicate that ground effects do not significantly affect the shock TOA for the steel configuration. The tungsten shot exhibits the opposite behavior expected if observing ground effects retarding the shock traveling over the pressure probes. The image analysis shows a slower shock traveling away normal to the ground. The pressure transducers were oversized for the first particle liner shot (tungsten) and more accurately sized in the subsequent shots (steel). It is likely that the pressure probes lag in the tungsten shot since they are responding to a relatively small pressure wave.

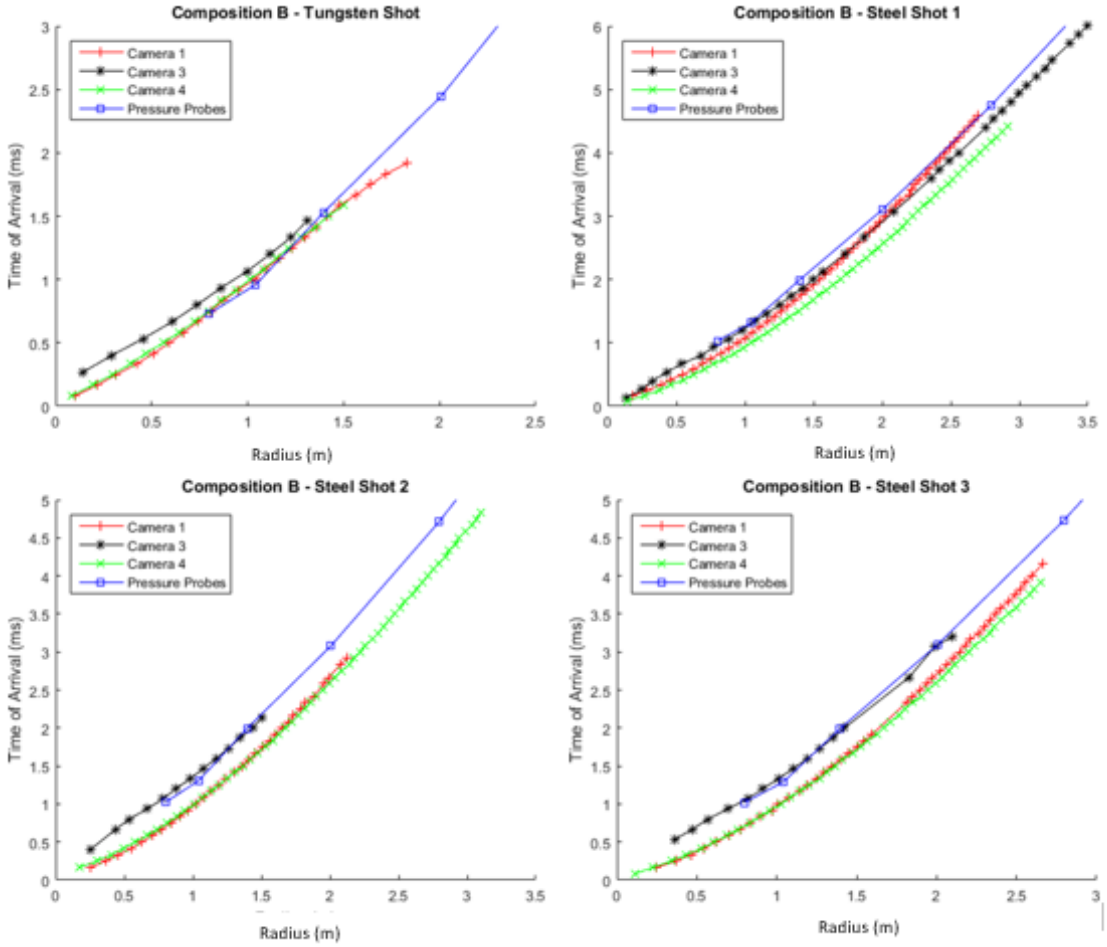

Figure 16. Image analysis results for shock tracking

Finally, Figure 17 presents an aggregate plot of shock TOA including the pressure probe and camera 3 results for all four particle liner shots. Cameras 1 and 4 have been discarded per the discussion above. The image analysis provides an excellent complement to the pressure probe data, especially by providing data at many more points than the four positions offered by the pressure probes.

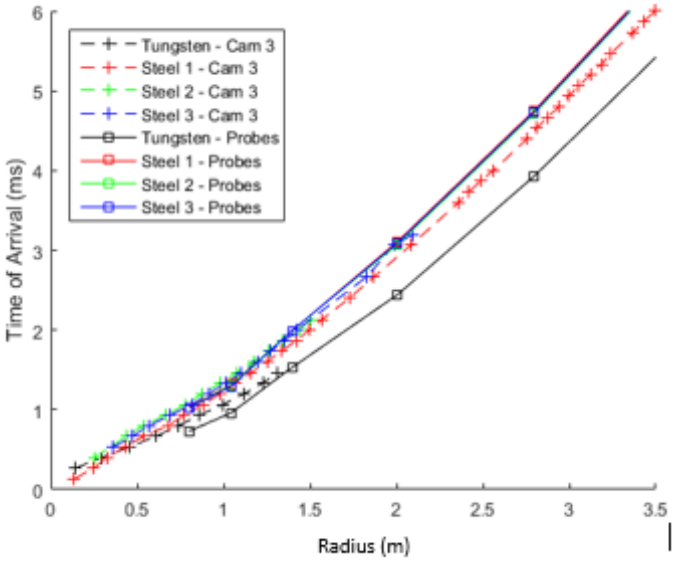

Figure 17. Aggregate plot of shock time of arrival for all four particle liner shots

V. CONCLUSION

The macroscale experimental data for the simple multiphase configuration tested here provides an excellent source of validation data for high fidelity multiphase models. Extensive uncertainty quantification of the experimental configuration has been performed a priori to equip the analyst with more information than typically available for validation experiments. Particle density, particle diameter, and charge characterization have been measured for six explosive shots including two bare charges, three steel liners, and a single tungsten liner. Compoarison of pressure data for the legacy and current bare charges shows close agreement and allows the uncertainty analysis to leverage four total shots for the baseline configuration. The effect of case notching was investigated for the steel liner configurations and shown to have no effect for the casing material used. High speed video from four different viewpoints provide shock location as a function of time. Pressure histories provide further validation data at 54 radial locations around the charge, where the pressure probes provide a redundant source of shock time of arrival. Additional analysis and comparison to simulation results are planned as future work for this project.

ACKNOWLEDGEMENTS

The authors would like to acknowledge the efforts of the test team at the AFRL/RW AWEF and Lt. Sarah Folse for test support. Additionally, the authors would like to thank the energetic materials processing team at the AFRL/RW HERD for the extra measurements taken to ensure proper uncertainty quantification.

REFERENCES

1 Oberkampf, W. L., "What are validation experiments?," *Experimental Techniques*, vol. 25, May 2001, pp. 35–40.

2 Sun, M., Saito, T., Takayama, K., and Tanno, H., "Unsteady drag on a sphere by shock wave loading," *Shock Waves*, vol. 14, 2005, pp. 3–9.

3 Tanno, H., Komuro, T., Takahashi, M., Takayama, K., Ojima, H., and Onaya, S., "Unsteady force measurement technique in shock tubes," *Review of Scientific Instruments*, vol. 75, 2004, pp. 532–536.

4 Tanno, H., Itoh, K., Saito, T., Abe, A., and Takayama, K., "Shock wave interaction with a sphere in a shock tube," *Shock Waves*, 2004, pp. 483–497.

5 Jourdan, G., Houas, L., Igra, O., Estivalezes, J.-L., Devals, C., and Meshkov, E. E., "Drag coefficient of a sphere in a non-stationary flow: new results," *Proceedings of the Royal Society A: Mathematical, Physical and Engineering Sciences*, vol. 463, Dec. 2007, pp. 3323–3345.

6 Britan, A., Elperin, T., Igra, O., and Jiang, J. P., "Acceleration of a sphere behind planar shock waves," *Experiments in Fluids*, vol. 20, Dec. 1995, pp. 84–90.

7 Wagner, J. L., Beresh, S. J., Kearney, S. P., Pruett, B. O. M., and Wright, E. K., "Shock tube investigation of quasi-steady drag in shock-particle interactions," *Physics of Fluids*, vol. 24, 2012.

8 Hughes, K., Diggs, A., Littrell, D., Balachandar, S., Haftka, R. T., Kim, N. H., Park, C., and DelCambre, M., "Uncertainty Quantification of Experiments on a Small Number of Explosively-Driven Particles," *55th AIAA Aerospace Sciences Meeting*, Reston, Virginia: American Institute of Aeronautics and Astronautics, 2017, pp. 1–14.

9 DeMauro, E. P., Wagner, J. L., DeChant, L. J., Beresh, S. J., Farias, P., Turpin, A., Sealy, W., Albert, S., and Sanderson, P., "Measurements of the Initial Transient of a Dense Particle Curtain Following Shock Wave Impingement," *55th AIAA Aerospace Sciences Meeting*, Grapevine, Texas: American Institute of Aeronautics and Astronautics, 2017, pp. 1–13.

10 Wagner, J. L., Beresh, S. J., Kearney, S. P., Trott, W. M., Castaneda, J. N., Pruett, B. O., and Baer, M. R., "A multiphase shock tube for shock wave interactions with dense particle fields," *Experiments in Fluids*, vol. 52, 2012, pp. 1507–1517.

11 Kellenberger, M., Johansen, C., Ciccarelli, G., and Zhang, F., "Dense particle cloud dispersion by a shock wave," *Shock Waves*, vol. 23, 2013, pp. 415–430.

12 Frost, D. L., Ornthanalai, C., Zarei, Z., Tanguay, V., and Zhang, F., "Particle momentum effects from the detonation of heterogeneous explosives," *Journal of Applied Physics*, vol. 101, Jun. 2007, p. 113529.

13 Frost, D. L., Grégoire, Y., Petel, O., Goroshin, S., and Zhang, F., "Particle jet formation during explosive dispersal of solid particles," *Physics of Fluids*, vol. 24, Sep. 2012, p. 91109.

14 Frost, D. L., Zarei, Z., and Zhang, F., "Instability of Combustion Products Interface from Detonation of Heterogeneous Explosives," *International Colloquium on the Dynamics of Explosions and Reactive Systems*, 2005, pp. 1–6.

15 Zhang, F., Frost, D. L., Thibault, P. a., and Murray, S. B., "Explosive dispersal of solid particles," *Shock Waves*, vol. 10, Jan. 2001, pp. 431–443.

16 Barreto, M., Ohrt, A., and Davis, R., *The AFRL Blastpad 2015 : Refinements in Design and Procedures*, Eglin AFB, FL: 2015.

17 Zhang, F., Ripley, R. C., Yoshinaka, A., Findlay, C. R., Anderson, J., and von Rosen, B., "Large-scale spray detonation and related particle jetting instability phenomenon," *Shock Waves*, vol. 25, 2015, pp. 239–254.

18 Dobratz, B. M., and Crawford, P. C., "LLNL Explosives Handbook - Properties of Chemical Explosives and Explosive Stimulants," Jan. 1985.

DISTRIBUTION LIST

AFRL-RW-EG-TR-2018-029

*Defense Technical Info Center
8725 John J. Kingman Rd Ste 0944
Fort Belvoir VA 22060-6218

AFRL/RWMW (1)
AFRL/RWORR (STINFO Office) (1)